Dissociative and diffractive scattering of H-2 from Pt(111): A four-dimensional quantum dynamics study

Pijper, E.; Kroes, G.; Olsen, R.A.; Baerends, E.J.

published in
Journal of Chemical Physics
2002

DOI (link to publisher)
10.1063/1.1475744

document version
Publisher's PDF, also known as Version of record

Dissociative and diffractive scattering of H_2 from Pt(111): A four-dimensional quantum dynamics study

E. Pijper and G. J. Kroes[a)]
Leiden Institute of Chemistry, Gorlaeus Laboratories, Leiden University, P.O. Box 9502, 2300 RA Leiden, The Netherlands

R. A. Olsen and E. J. Baerends
Theoretische Chemie, Vrije Universiteit, De Boelelaan 1083, 1081 HV Amsterdam, The Netherlands

(Received 2 January 2002; accepted 12 March 2002)

Following earlier three-dimensional (3D) calculations, we present results of four-dimensional (4D) calculations on dissociative and diffractive scattering of H_2 from Pt(111) by extending the 3D model with a second degree of freedom parallel to the surface. A 4D potential energy surface (PES) is constructed by interpolating four 2D PESs obtained from density-functional theory calculations using the generalized gradient approximation and a slab representation of the metal surface. The 4D calculations show that out-of-plane diffraction is much more efficient than in-plane diffraction, providing a partial explanation for the paradox that diffraction experiments measure little in-plane diffraction, whereas experiments on reaction suggest the surface to be corrugated. Calculations for off-normal incidence of $v=0$ H_2 show that, in agreement with experiment, initial parallel momentum inhibits dissociation at low normal translational energies, and enhances reaction for higher energies. Our 4D calculations also show that the reaction of initial $v=1$ H_2 is vibrationally enhanced with respect to $v=0$ H_2, as was found in the 3D model, even though $H_2+Pt(111)$ is an early barrier system. © *2002 American Institute of Physics.* [DOI: 10.1063/1.1475744]

I. INTRODUCTION

Scattering of H_2 from Pt(111) is of interest for several reasons (see Ref. 1 and references therein). For instance, in hydrogenation reactions Pt serves as a catalyst, providing an efficient environment for reactions involving H atoms adsorbed on the surface.[2–4] An issue which has received much attention for Pt(111) is how important defect sites are for the dissociation of H_2.[2–9] Furthermore, the effect that alloying the surface with an unreactive metal (Sn) has on the dissociation of H_2 has also been investigated for Pt(111).[10]

The most relevant aspect of the $H_2+Pt(111)$ system to the present study is a controversy regarding how corrugated the surface looks to H_2. Luntz *et al.*[11] concluded from their results on reaction of D_2 on Pt(111) that the potential must be rather corrugated, since their data showed that initial parallel momentum had a large effect on the reaction probability, i.e., normal energy scaling was not obeyed. On the other hand, Cowin *et al.*,[12] when looking at rotationally inelastic scattering of HD from Pt(111), found very little diffraction, suggesting that the potential must be rather flat.

This controversy was also addressed in a previous paper[1] on $H_2+Pt(111)$ where results of two-dimensional (2D) and three-dimensional (3D) calculations were presented. In the 3D calculations a model was employed in which the molecular degrees of freedom were the center-of-mass distance to the surface Z, the internuclear distance r, and one translational degree of freedom parallel to the surface x. The results showed that the reaction of H_2 on Pt(111) is vibrationally enhanced. This was unexpected since all barriers to dissociation are early, implying that vibrational energy cannot have been released through an increase of the reduced mass,[13] which is a well-known effect by which the reaction is enhanced for late barriers.[14] Our analysis showed that the force constant associated with the vibration in the entrance channel decreased as the molecule approached the barrier. The vibrational energy that is hereby released goes partly into translation along Z, thereby enhancing reaction. A similar mechanism had previously been found for $H_2+Pd(100)$.[15]

We also found that normal energy scaling was not obeyed, in agreement with experiment.[11] On the other hand, our calculations showed substantial diffraction, in disagreement with experiment.[12]

In the present paper we extend the 3D model to a four-dimensional (4D) model by including a second translational degree of freedom, y, for motion parallel to the surface. In our 4D model, the molecule is always oriented parallel to the surface but its azimuthal orientation depends on the surface site over which it dissociates. Questions that we will address are whether the previous results of the 3D calculations still hold. It is expected that vibrational enhancement will also be found in the 4D calculations, and that the reaction will not scale with the normal energy. These predictions are made on the basis that in the 4D calculations no new surface sites are present that were not present in the 3D calculations. However, as stated before, we expect that diffraction will be less efficient due to the smaller surface lattice constant in the 4D model.[1] In the 3D model the surface lattice constant L was equal to the separation of the two top sites that are furthest apart in the diamond shaped surface unit cell (9.08 bohr). In

a)Electronic mail: g.j.kroes@chem.leidenuniv.nl

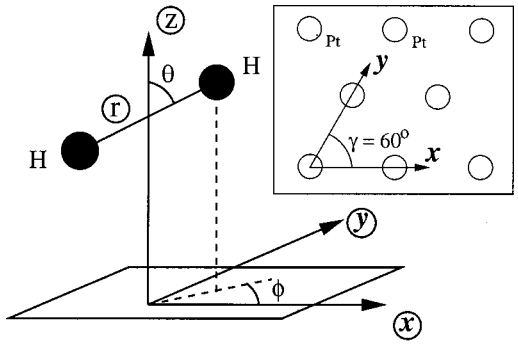

FIG. 1. Shown is the coordinate system of H_2 with respect to a fixed Pt(111) surface. The encircled coordinates represent the degrees of freedom treated in the present 4D calculations. The inset shows the nonorthogonal x and y coordinates of the Pt(111) face, γ being the skewing angle.

the 4D model the correct surface lattice constant is used, given by the smallest distance between two top sites in the (111) face of Pt (5.24 bohr). Since momentum parallel to the surface can only change by discrete amounts of $\Delta K = 2\pi/(L \sin\gamma)$, with $\gamma = 60°$ for the (111) surface, and the associated energy changes are proportional to $(\Delta K)^2$, the use of a too large lattice constant (and ignoring the factor $\sin\gamma$) is expected to lead to too efficient diffraction in the 3D model.

We will present results for normal and off-normal incidence, and look at the effect of corrugation on diffraction and dissociation. All degrees of freedom in the 4D model are treated quantum mechanically. The calculations are performed using the time-dependent wave packet (TDWP) method.[16] We use a 4D potential energy surface (PES) that was obtained from an interpolation of four 2D PESs. Each 2D PES is, in turn, a spline interpolation of potential points calculated with density-functional theory (DFT), employing the generalized gradient approximation (GGA)[17,18] and using a slab representation of the surface.[19]

This paper is organized as follows. Because the wave packet method and propagation method used are extensively described in Ref. 1, Sec. II will mostly focus on how these methods are extended to a skewed surface unit cell. Also discussed in Sec. II is the construction of the 4D PES. In Sec. III results of 4D calculations are presented. In Sec. III A reaction for normal incidence is discussed. Results of reaction and diffraction for off-normal incidence are presented in Secs. III B and III C, respectively. The comparison with experiment is discussed in Sec. III D for reaction and in Sec. III E for diffraction, followed by conclusions in Sec. IV.

II. THEORY

A. Dynamical model

The $H_2 + Pt(111)$ system is treated within a four-dimensional (4D) model. The four degrees of freedom are indicated in Fig. 1. They are the center-of-mass distance to the surface Z, the H–H internuclear distance r, and two translational degrees of freedom for motion parallel to the surface x and y. The lateral coordinates x and y are nonorthogonal, or skewed coordinates, meaning that the unit vectors associated with these coordinates are nonorthogonal.

As usual, two approximations are made.[20,21] First, the Born–Oppenheimer approximation is made to decouple the motion of the electrons from the nuclear motion, restricting the reaction to take place on the ground-state PES only. In this way, electron–hole pair excitations are neglected. Second, the Pt atoms are fixed to their equilibrium position in the lattice, making energy exchange with the surface through phonons impossible.

The Hamiltonian for the nuclear motion of the system using skewed coordinate axes is given by[22,23]

$$\hat{H} = -\frac{1}{2M}\frac{\partial^2}{\partial Z^2} - \frac{1}{2\mu}\frac{\partial^2}{\partial r^2} - \frac{1}{2M\sin^2\gamma} \times \left[\frac{\partial^2}{\partial x^2} - 2\cos\gamma\frac{\partial}{\partial x}\frac{\partial}{\partial y} + \frac{\partial}{\partial y^2}\right] + V_{4D}(Z,r,x,y), \quad (1)$$

where atomic units have been used. The masses M and μ are the total mass and reduced mass of H_2, respectively, and γ is the angle between the x and y axes as indicated in Fig. 1. For the (111) face of Pt, $\gamma = 60°$. The 4D interaction potential is represented by V_{4D}. It is an interpolation of four 2D PESs obtained from density functional theory calculations (see Sec. II C).

Reaction probabilities and scattering probabilities are calculated using a time-dependent wave packet (TDWP) method,[16] as discussed in more detail in Ref. 1 for the 3D model. The 4D model is a simple extension of this. Briefly, a Gaussian wave packet[24] that is initially located far from the surface is propagated in time according to the time-dependent Schrödinger equation. It collides with the surface, where a part reacts and a part reflects. The reflected part is analyzed at a value Z_∞ where the interaction with the surface is negligible, to obtain probabilities for vibrationally elastic and vibrationally inelastic diffraction. The reaction probability for a total collision energy E_i is then determined by computing the total reflection probability for E_i by summing the scattering probabilities and subtracting the sum from 1. The part of the wave packet that is reflected is absorbed beyond Z_∞ using an optical potential.[25] An optical potential is also used to absorb the part of the wave packet that has reacted, i.e., for which the internuclear separation is larger than some value r_d. The wave packet is propagated using the split operator propagator,[26] and analyzed using a formalism developed by Balint-Kurti *et al.*[27–29] The wave function is represented on grids in Z, r, x, and y using a direct product discrete variable representation (DVR)[30] with constant grid spacings ΔZ, Δr, Δx, and Δy.

B. Treatment of the skewed surface unit cell

The skewed nature of the unit cell and, consequently, the use of nonorthogonal coordinates require special attention. Below we describe how to deal with a general skewed unit cell. Since the use of nonorthogonal coordinates x and y does not affect the description of rotation and vibration, we will focus only on the translational coordinates. Part of the discussion pertaining to the description of crystal surfaces can be found in many books on Solid State Physics, for instance Refs. 31 and 32.

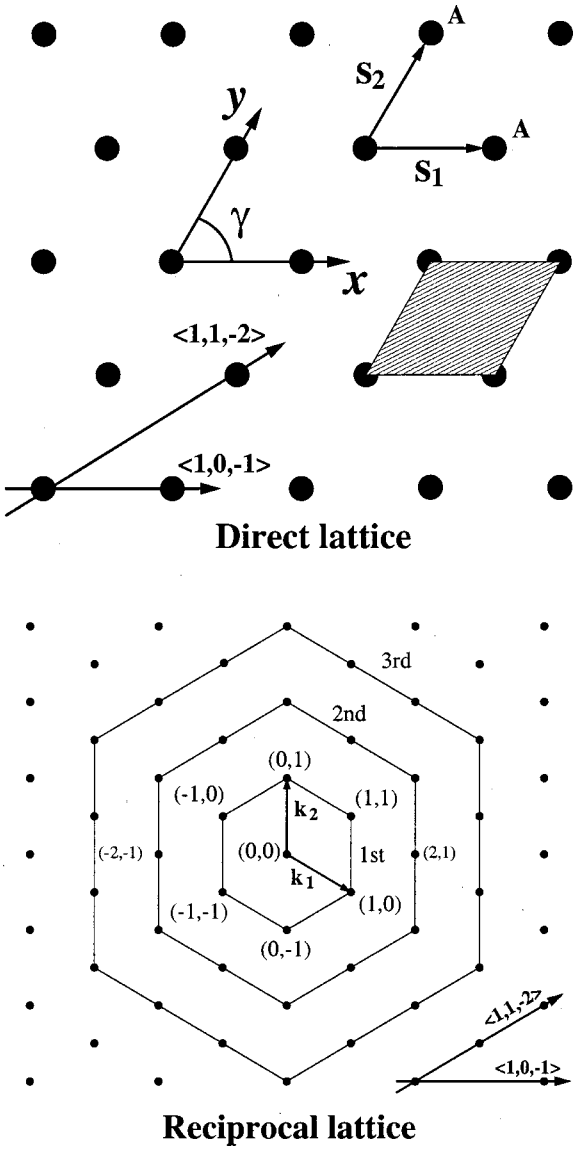

FIG. 2. A (111) lattice consisting of atoms A is shown in the upper plot. The angle γ is the skewing angle, and $\mathbf{s}_1$ and $\mathbf{s}_2$ are the primitive vectors that span the surface unit cell (shaded area). In the lower plot the reciprocal lattice and its primitive vectors are depicted. The lattice points of the reciprocal lattice correspond to wave vectors $\mathbf{K}$ that are a solution of Eq. (3). The concentric hexagons indicate how diffraction order is defined for the (111) lattice. The $\langle 101\rangle$ and $\langle 112\rangle$ directions have been indicated in both plots.

The position vector of an atom in a crystal surface plane, with respect to an arbitrary origin $\mathcal{O}$, is given by

$$\mathbf{R}=p\mathbf{s}_1+q\mathbf{s}_2, \tag{2}$$

where p and q range through all integral values. The vectors $\mathbf{s}_1$ and $\mathbf{s}_2$ generate the complete lattice of surface atoms and are the called the primitive vectors of a Bravais lattice.[31,32] They can be chosen in many different ways. For surface scattering calculations the most convenient choice is shown in Fig. 2 for a (111) surface lattice of atoms.

Bloch's theorem[31,32] states that, in scattering of particles from a crystal surface, only well defined parallel translational momentum states (diffraction states) are allowed due to the periodicity of the surface. These diffraction states are closely related to the reciprocal lattice of the crystal surface (the exact relation follows below), which is the set of all wave vectors $\mathbf{K}$ that satisfy

$$\exp(i\mathbf{K}\cdot\mathbf{R})=1, \tag{3}$$

for all $\mathbf{R}$ defined in Eq. (2). Wave vectors $\mathbf{K}$ satisfying Eq. (3) describe plane waves that have the periodicity of the surface. It can be shown that the set of solutions $\mathbf{K}$ of Eq. (3) also produces a Bravais lattice and can, therefore, be expressed as

$$\mathbf{K}=n\mathbf{k}_1+m\mathbf{k}_2, \tag{4}$$

where $\mathbf{k}_1$ and $\mathbf{k}_2$ are primitive vectors of the reciprocal lattice, and n and m range through all integral values. In Fig. 2, the reciprocal lattice corresponding to the (111) lattice is also shown. The subscripts "1" and "2" do *not* imply that $\mathbf{k}_1$ and $\mathbf{k}_2$ lie along the same direction as $\mathbf{s}_1$ and $\mathbf{s}_2$, respectively. Only for a square or rectangular unit cell will this be the case. The subscripts serve only a notational purpose.

Substituting Eqs. (2) and (4) into Eq. (3), we obtain an equation that must be identically satisfied for *all* p, q, n, and m. This leads to the following four constraints on $\mathbf{k}_i$ and $\mathbf{s}_j$:

$$\mathbf{k}_i\cdot\mathbf{s}_j=\delta_{ij}2\pi l, \tag{5}$$

where i and j can be 1 or 2, δ_{ij} is the Kronecker delta symbol, and l can be any integer value. By choosing $l=1$, a particular choice of the $\mathbf{k}_i$ is made. Solutions for $l\neq 1$ will yield $\mathbf{k}_i'=l\mathbf{k}_i$, i.e., the difference is only a multiplicative constant. The choice $l=1$ then corresponds to vectors $\mathbf{k}_i$ that are shortest in length.

Equation (5) shows that $\mathbf{k}_1\perp\mathbf{s}_2$ and $\mathbf{k}_2\perp\mathbf{s}_1$. The other two constraints define the length and direction of $\mathbf{k}_1$ and $\mathbf{k}_2$. The parallel momentum of a diffraction state is then given by

$$\mathbf{K}_{nm}^f=\mathbf{K}^0+n\mathbf{k}_1+m\mathbf{k}_2, \tag{6}$$

where n and m again range through all integral values and are called the diffraction quantum numbers. The vectors $\mathbf{K}^0$ and $\mathbf{K}^f$ represent the initial and final momentum parallel to the surface, respectively. The length of $\mathbf{k}_i$ is the minimum amount of momentum that can be gained or lost in the direction of $\mathbf{k}_i$, and is given by

$$\Delta k_i=\frac{2\pi}{|\mathbf{s}_i|\sin\gamma}. \tag{7}$$

The scattering wave function can be written as (Bloch's theorem)

$$\Psi_s(\mathbf{r})=\sum_{nm}\alpha_{nm}(Z)\exp[i\mathbf{K}_{nm}^f\cdot\mathbf{R}], \tag{8}$$

where $\mathbf{K}_{nm}^f$ is given by Eq. (6), and the summation is over the diffraction channels (n,m). The coefficient $\alpha_{nm}(Z)$ determines the contribution of diffraction state (n,m) to the scattering wave function in Z. In expression (8), $\mathbf{r}$ is a three-dimensional coordinate vector, and $\mathbf{R}$ a vector that depends on x and y only. To compute the inner product, the vectors $\mathbf{K}_{nm}^f$ and $\mathbf{R}$ are replaced by an appropriate representation. The obvious choice is to represent $\mathbf{R}$ using the skewed coordinate system of Eq. (2)

$$\mathbf{R}=x\hat{\mathbf{s}}_1+y\hat{\mathbf{s}}_2, \tag{9}$$

where $\hat{\mathbf{s}}_1$ and $\hat{\mathbf{s}}_2$ are the unit vectors corresponding to the primitive vectors $\mathbf{s}_1$ and $\mathbf{s}_2$, respectively. The vector $\mathbf{K}^f_{nm}$ is represented using the skewed coordinate system of Eq. (6)

$$\mathbf{K}^f_{nm}=(K^0_1+n\Delta k_1)\hat{\mathbf{k}}_1+(K^0_2+m\Delta k_2)\hat{\mathbf{k}}_2, \tag{10}$$

where $\hat{\mathbf{k}}_1$ and $\hat{\mathbf{k}}_2$ are the unit vectors corresponding to the primitive vectors $\mathbf{k}_1$ and $\mathbf{k}_2$, respectively. The quantities K^0_1 and K^0_2 refer to the components of the initial momentum $\mathbf{K}^0$ along $\hat{\mathbf{k}}_1$ and $\hat{\mathbf{k}}_2$, respectively. Using Eqs. (5), (7), (9), and (10), expression (8) can be written as

$$\Psi_s(\mathbf{r})=\exp[i\sin\gamma(K^0_1x+K^0_2y)]$$

$$\times\sum_{nm}\alpha_{nm}(Z)\exp[i(n\Delta\kappa_1x+m\Delta\kappa_2y)], \tag{11}$$

where $\Delta\kappa_1=2\pi/|\mathbf{s}_1|$ and $\Delta\kappa_2=2\pi/|\mathbf{s}_2|$. The term in front of the summation describes a plane wave corresponding to the incoming particle, and is important in calculations for off-normal incidence.[33] The summation is over the diffraction channels (n,m), and its *form* is independent of the shape of the unit cell. Therefore, a code that works for a (100) unit cell can be very easily modified to also work for a (111) unit cell.

In discussing the results the concept of diffraction order will often be used. For a square unit cell, the diffraction order P has sometimes been defined as $P=|n|+|m|$.[34] Using this definition, the first-order diffraction channels (1,0), $(-1,0)$, (0,1) and $(0,-1)$ correspond to a momentum change of one quantum Δk. Looking at the reciprocal lattice, and connecting the first-order diffraction channels, the Pth diffraction orders then consists of all diffraction channels on the Pth concentric square. For the (111) surface, we define the diffraction order in a similar way, as shown in Fig. 2: The first-order diffraction channels correspond to a momentum change Δk. The Pth diffraction order then consists of all diffraction channels on the Pth concentric hexagon in Fig. 2. When we mention diffraction order in discussing our results below, this is the definition used, unless explicitly stated otherwise.

C. The PES

The potential energy surface used in the calculations is a four-dimensional interpolation of four 2D PESs obtained from density-functional theory (DFT). The DFT calculations were based on the generalized gradient approximation (GGA)[17,18] and used a 3 layers slab representation[19,35] of the surface with a 2×2 unit cell.[36] Relativistic effects, which are important for Pt, are taken into account by the zero-order regular approximation (ZORA).[37] Figure 3 shows these four 2D PESs. Each 2D PES is a bicubic spline interpolant of between 50 and 60 DFT points. In the DFT calculations, the H_2 molecule is always parallel to the surface. Its azimuthal orientation varies with x and y. The top site PES corresponds to the coordinates $(x=0,y=0)$ and $\phi=120°$ (see also Fig. 2). The bridge site PES corresponds to coordinates $(x=L/2,y=0)$ and $\phi=0°$. The fcc PES site corresponds to $(x=L/3,y=L/3)$ and $\phi=120°$. The PES for the fourth site, the so-called t2f site, corresponds to $(x=L/6,y=L/6)$ and $\phi=120°$. The azimuthal angle ϕ is defined with respect to the x axis (see Fig. 1). The surface lattice constant L is the distance between two neighboring Pt surface atoms: $L=5.24$ bohr.

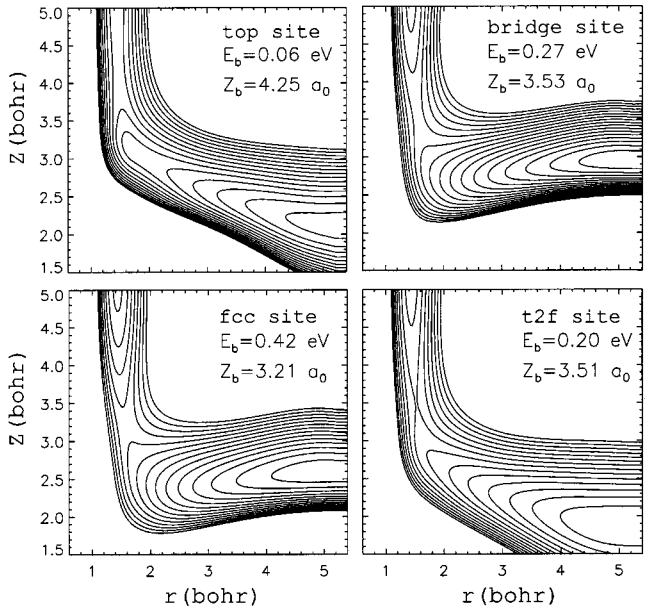

FIG. 3. Shown are four 2D PESs computed by DFT and used to construct a 4D PES (Ref. 36). The level spacing is 0.1 eV. Indicated in each plot is the barrier height E_b and distance of the barrier to the surface, Z_b. The molecule is always parallel to the surface. The azimuthal orientation of H_2 varies per site.

To obtain a 4D PES, the four 2D PESs are interpolated using an analytical expression for the 4D PES. The interpolation assumes C_{6v} symmetry, but the (111) face is in reality only of C_{3v} symmetry. For instance, the 2D PESs for the hollow fcc sites and hcp sites are not equal. However, DFT calculations for these sites show that assuming C_{6v} symmetry represents a reasonable approximation.[36,38]

The interpolation is done by use of the following analytical expression that satisfies C_{6v} symmetry:

$$\begin{aligned}V(Z,r,x,y)=&\,c_0(Z,r)H_{00}(x,y)\\&+c_1(Z,r)H_{10}(x,y)+c_2(Z,r)H_{21}(x,y)\\&+c_3(Z,r)H_{20}(x,y),\end{aligned} \tag{12}$$

where

$$\begin{aligned}H_{00}&=\frac{1}{L}\\H_{10}&=\frac{1}{L}\sqrt{\frac{2}{3}}(\cos(Gx)+\cos(Gy)+\cos(Gx+Gy))\\H_{21}&=\frac{1}{L}\sqrt{\frac{2}{3}}(\cos(2Gx+Gy)+\cos(Gx+2Gy)\\&\quad+\cos(Gx-Gy))\end{aligned} \tag{13}$$

TABLE I. List of input parameters and their values in the 4D calculation for dissociation of $v=0$ H_2 at normal incidence, for the energy ranges indicated. Values are in atomic units unless indicated otherwise.

	Energy range	
Parameter	[0.05–0.153]	[0.147–0.45]
Initial wave packet		
Width ξ (bohr)	1.453	0.847
Initial position Z_0	10.25	8.75
Average initial momentum k_{Z_0}	5.051	8.662
Grid parameters		
Z_i	−1.0	same
N_Z	96	same
r_i	0.4	same
N_r	54	same
N_X	24	same
N_Y	24	same
N_Z^{sp}, # grid points specular grid	144	same
Grid spacing ΔZ	0.15	same
Grid spacing Δr	0.15	same
Lattice constant L	5.24	same
Time propagation		
Size time step Δt	2.5	5.0
Number of time steps	12 000	6000
Optical potential in Z		
Initial value of range $Z_{\min}$	6.80	same
Proportionality constant A_2	0.0031	0.0037
Range L_O	6.45	same
Optical potential in r		
Initial value of range $r_{\min}$	4.15	same
Proportionality constant A_2	0.021	0.0095
Range L_O	4.2	same
Other parameters		
Analysis value Z_∞	6.80	same

$$H_{20}=\frac{1}{L}\sqrt{\frac{2}{3}}(\cos(2Gx)+\cos(2Gy)+\cos(2Gx+2Gy)).$$

Here, $G=2\pi/L$.

Equations (13) define a set of four equations with four unknowns, $c_i(Z,r)$. These can be obtained from the four 2D PESs calculated by DFT using simple algebra. A simple inversion of Eq. (13) yields a PES with artificial oscillations. Fortunately, the artefacts only occur in the exit channel, for H–H separations much larger than found at the barriers to reaction, i.e., for $r>3.0\,a_0$. To avoid the occurrence of artificial oscillations in the PES that may hamper the calculation of reaction probabilities, we set the potential constant in the exit channel for $r>3.0a_0$ according to

$$V_{2D}(Z,r>3.0)=V_{2D}(Z,r=3.0). \tag{14}$$

To make sure that only the exit channel is affected we also use a switching function between $Z=2.5$ and $Z=3.0$ bohr in the same way as was done previously for the 3D PES.[1] The 4D interpolation was then repeated by again solving for the $c_i(Z,r)$ in Eq. (13).

D. Computational details

Table I lists the relevant parameters used in the calculation of $v=0$ H_2 for normal incidence. To cover the collision energy range $E_i=0.05-0.45$ eV, two wave packet calculations were done for two separate energy ranges. This procedure is followed to avoid problems which could result from the interaction of low-translational energy components in the wave packet with the optical potential if only one broad Gaussian initial wave packet would be used to cover $E_i=0.05-0.45$ eV for motion in Z.

Calculations were also done for $v=1$ H_2 for normal incidence, and for $v=0$ H_2 for off-normal incidence. In these calculations the only parameters that needed to be changed in order to obtain convergence relative to the values used for $v=0$ H_2 for normal incidence (Table I), were the number of points in x and y. For all off-normal incidence calculations, $N_x=N_y=36$ was used. For initial $v=1$ H_2, $N_x=N_y=32$ was needed.

The projection operator formalism[39] was used to bring in the initial wave packet on a separate, long one-dimensional grid in order to be able to reduce the grid size in Z associated with the large scattering basis set.

To investigate reaction, calculations were performed for $E_\parallel=0.0533$, 0.16, and 0.48 eV. To investigate diffraction, additional calculations were performed for $E_\parallel=0.0348$ eV.

Probabilities $\geqslant 0.03$ are converged to within 1% of their absolute value. The convergence of probabilities smaller than 0.03 may not be as good but the absolute error is always smaller than 3×10^{-4}.

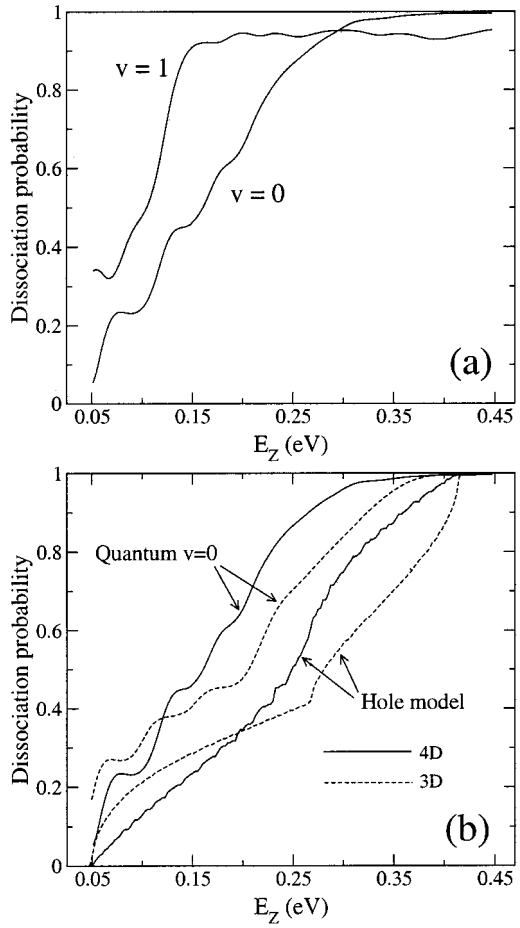

FIG. 4. Reaction probabilities of 4D quantum dynamics calculations for $v=0$ and $v=1$ H_2 on Pt(111) are shown (a). Results of the hole model are compared with the quantum results for $v=0$, for both the 3D and 4D model (b). Results are for normal incidence, and plotted as a function of the collision energy E_Z.

III. RESULTS AND DISCUSSION

Calculations have been done for normal and off-normal incidence. Results of calculations for normal incidence will be presented and discussed in Sec. III A. Section III B focuses on reaction for off-normal angles of incidence. In Sec. III C results of diffraction for off-normal angles of incidence are discussed. In Secs. III D and III E computational results for reaction and diffraction are compared with experiment.

A. Normal incidence

Figure 4(a) shows results of 4D calculations for dissociation of H_2 on Pt(111), for normal incidence. The results are for $v=0$ and $v=1$ H_2. At the lowest energy for which results have been obtained ($E_Z=0.05$ eV) the reaction probability is about 0.05, and it saturates for an energy of ~0.40 eV, where the probability is almost 1. The dissociation of initial $v=1$ H_2 shows vibrational enhancement with respect to $v=0$. For the lowest energy the dissociation probability for $v=1$ is enhanced by more than a factor 6. Such a large vibrational enhancement is unexpected for the $H_2+Pt(111)$ system[1] because it is an early barrier system. Vibrational enhancement is usually associated with late barrier systems like $H_2+Cu(100)$.[40,41] For these systems, as the molecule approaches the barrier, vibrational energy can be released to motion along the reaction path due to an increase of the reduced mass associated with the (vibrational) motion perpendicular to the reaction path.[14] In an early barrier system, however, there is little change in the reduced mass as the H_2 approaches the barrier. Consequently, any vibrational enhancement found for an early barrier system must be due to some other mechanism. For $H_2+Pt(111)$, vibrational energy release is due to a decrease of the force constant associated with the H_2 vibration as the molecule approaches the barrier.[1] The same mechanism is responsible for the vibrational enhancement of reaction in the early barrier system $H_2+Pd(100)$.[15] The same mechanism is also responsible for the efficient reaction of $v=0$ H_2 at low energies. The height of the lowest barrier of the 4D PES is 0.06 eV, found at the top site. Yet for a collision energy of 0.05 eV we find already a substantial reaction probability that cannot be entirely attributed to tunneling. Instead, zero-point vibrational energy is released in the same way as discussed for $v=1$ and flows towards other degrees of freedom, including motion along the reaction path.

Vibrational enhancement was not found in the seeded beam experiments of Luntz *et al.*[11] However, as discussed in Ref. 1, vibrational enhancement of reaction should be hard to measure in seeded beam experiments if the reaction of $v=0$ has a very low threshold.

To contrast the 4D results with those of the 3D calculations,[1] the 4D results for $v=0$ are compared with previous 3D results in Fig. 4(b). Concentrating on the $v=0$ results, the probability curves are seen to cross at a collision energy of ~0.12 eV. The origin of this crossing can be qualitatively understood from the hole model by considering the integrated barrier distribution[15]

$$P_b(E_Z)=\frac{1}{2\pi A}\int \Theta(E_Z-E_b(x,y))\mathrm{d}x\mathrm{d}y, \tag{15}$$

where A is the unit cell surface area, and $E_b(x,y)$ the barrier height of a 2D cut with fixed lateral coordinates (x,y). The function Θ is the Heavyside step function. The quantity $P_b(E)$ then measures the fraction of configuration space that is classically open for dissociation at a collision energy E_Z. Figure 4(b) also shows the results of a calculation of $P_b(E_Z)$ for the 3D and 4D PESs used. The classical behavior is indicated by the onset and saturation energies of the curves, which reflect the lowest and highest barrier towards dissociation. At ~0.20 eV the curves cross. For energies below 0.20 eV, P_b^{3D} is higher than P_b^{4D}. For higher energies it is the other way around. This indicates that up to a collision energies of 0.20 eV the fraction of the one-dimensional configuration space in X open for dissociation in the 3D model is larger than the fraction of the unit cell open for dissociation in the 4D model at the same collision energy. Not surprisingly, the quantum results show a similar trend, the only difference being the position of the crossing point, which is shifted towards lower energies due mostly to vibrational energy release as discussed above.

In Table II we present average barrier heights for the 3D and 4D model based on a weighted sum of the sites on which the interpolation is based, each time including an extra site in

TABLE II. The first column gives the barrier heights of the sites included in the interpolation of the 3D and 4D PES. Also given are average barrier heights, $\bar{E}_b$ for the 3D and 4D PES that represent the average over all barriers with an energy equal to and lower than the barrier height in that row, and obtained using the listed weights.

		3D		4D	
Site	E_b (eV)	Weight	$\bar{E}_b$ (eV)	Weight	$\bar{E}_b$ (eV)
Top	0.06	1/6	0.06	1/12	0.06
t2f	0.20	1/3	0.15	1/2	0.18
Bridge	0.27	1/6	0.18	1/4	0.21
fcc	0.42	1/3	0.26	1/6	0.24

increasing order of barrier height. Using a classical approach to reaction, in which reaction is possible for energies above the average barrier height, these average barrier heights suggest that for translational energies smaller than 0.21 eV, the 3D model is likely to react better than the 4D model. For translational energies larger than 0.24 eV, the 4D model is more likely to react better. This shows that a simple argument, based on weighted average barrier heights, can correctly predict the presence of a crossing of the 3D and 4D quantum calculations.

The hole model analysis can also be used to make a good choice for the parallel translational degree of freedom x in a model only treating one diffractive coordinate. If x is taken along $\langle 112 \rangle$ (as was done in Ref. 1), both the lowest barrier (top site) and the highest barrier (fcc site) can be sampled. This sampling cannot be realized if x is taken along the $\langle 101 \rangle$ direction. Such a model would lead to a reaction probability curve with a too small energy width.

B. Off-normal incidence: Reaction

Wave packet calculations for off-normal incidence present a problem when it comes to comparison with experiment. In experiments usually results are obtained for a fixed angle of incidence. However, from the point of view of computational expense, it is much cheaper to obtain results for a fixed initial momentum parallel to the surface. One wave packet calculation can provide results for a range of translational energies E_Z normal to the surface, but only for one initial parallel momentum $K_\parallel$. In such a calculation, the polar angles of incidence θ_i sampled depend on the initial momenta $\mathbf{K}_Z$, as $\theta_i = \tan^{-1}(K_\parallel / K_Z)$. (Here, θ_i is measured with respect to the surface normal such that $\theta_i = 0$ corresponds to normal incidence.) However, the notion of one incidence angle to label the results of a set of calculations is useful and intuitive. We, therefore, introduced the angle ϑ_i and defined it as[1]

$$\vartheta_i = \tan^{-1}(\sqrt{E_\parallel / E_0}), \tag{16}$$

where $E_\parallel$ is the energy corresponding to the initial parallel momentum $K_\parallel$, and E_0 the dynamical barrier height for normal incidence. (The dynamical barrier height is defined as the translational energy E_Z for which the dissociation probability first becomes half its saturation value.) For the present 4D calculations, $E_0 = 0.160$ eV for $v = 0$ [see Fig. 4(a)]. The

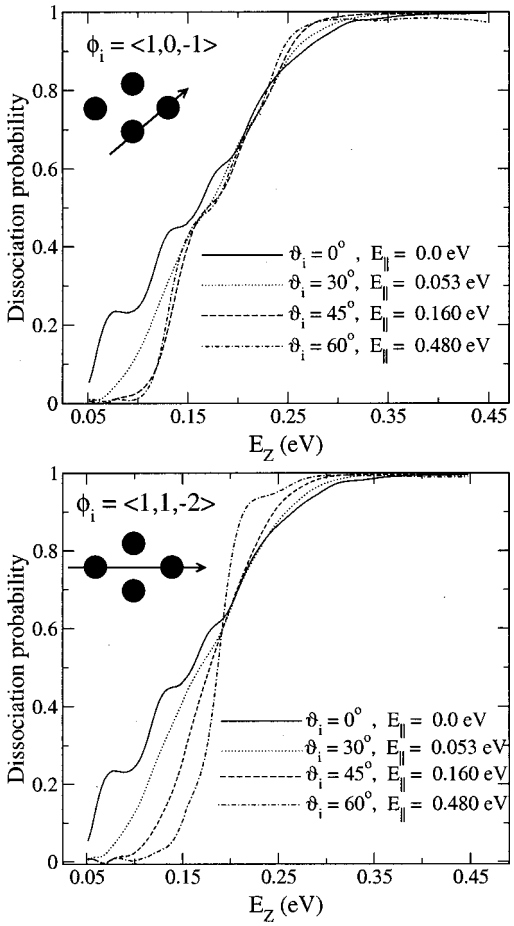

FIG. 5. Reaction probabilities of 4D quantum dynamics calculations for $v = 0$ H_2 are shown for four initial parallel translational energies, for the $\langle 101 \rangle$ and $\langle 112 \rangle$ incidence directions. The results are plotted as functions of the normal collision energy E_Z. The angle ϑ_i corresponds to the actual angle of incidence θ_i if $E_Z = E_0$, E_0 being the dynamical barrier height of $v = 0$ H_2 for normal incidence ($E_0 = 0.16$ eV).

angle ϑ_i and the initial parallel energy $E_\parallel$ will be used for labeling figures. If $E_Z = E_0$, then $\theta_i = \vartheta_i$. If $E_Z < E_0$, $\theta_i > \vartheta_i$, and if $E_Z > E_0$, $\theta_i < \vartheta_i$.

Calculations were done for two incidence directions, $\langle 101 \rangle$ and $\langle 112 \rangle$, and several initial parallel momenta corresponding to energies $E_\parallel = 0$, 0.0533, 0.160, and 0.480 eV. The angle ϑ_i varies between 0° and 60°. The results are presented in Fig. 5. Obviously, normal energy scaling is not obeyed, since parallel momentum has a large effect on the dissociation probability for both incidence directions. The effect of increasing parallel momentum is largest for incidence along the $\langle 112 \rangle$ direction. For both incidence directions initial parallel momentum inhibits dissociation for E_Z up to ~0.20 eV. However, for incidence along $\langle 101 \rangle$ and $E_\parallel \geqslant 0.16$ eV, the dependence of the dissociation probability on $E_\parallel$ is small. This is in contrast with incidence along $\langle 112 \rangle$ where increasing $E_\parallel$ beyond 0.16 eV still has a large effect on the dissociation probability. For energies E_Z larger than 0.20 eV initial parallel momentum enhances dissociation for both directions, but for the $\langle 101 \rangle$ direction the effect is again much less pronounced than for $\langle 112 \rangle$ for $E_\parallel \geqslant 0.16$ eV.

The effect of initial parallel momentum on the dissocia-

tion has been studied in detail by Darling and Holloway,[42] and Gross.[43] They employed a model potential that considered three molecular degrees of freedom: The center-of-mass distance from the surface *Z*, the inter-atomic distance *r* and one lateral surface degree of freedom *X*. In their study the effect of parallel momentum on dissociation was investigated and discussed for an energetically corrugated PES (variation of the barrier height but not of the distance of the barrier to the surface) and for a geometrically corrugated PES (variation of the barrier distance to the surface but not of the height). As discussed by Darling and Holloway, the case of the energetically corrugated PES is most relevant to $H_2+Pt(111)$.[42]

It was found that for an energetically corrugated PES initial parallel momentum inhibits dissociation at low normal translational energies[42,43] and enhances it for high normal translational energies.[43]

An explanation for the behavior observed in the low-energy regime was first given by Darling and Holloway.[42] Briefly, the initial parallel momentum will tend to sweep the molecule across the unit cell. Before it has had a chance to dissociate over a low barrier site, it can encounter a high barrier site from which it can be scattered back into the gas phase. The higher its initial parallel momentum, the more likely that it will encounter such a high barrier site, and, therefore, the smaller the probability of reaction. This effect is largest at low normal translational energies. By increasing the translational energy normal to the surface, the molecule will spend less time in the interaction region and has, on average, a better chance to dissociate over a low barrier site before it encounters a high barrier. Of course, increasing the normal energy also helps increasing the reaction probability because more sites become available for reaction.

Gross[43] has also investigated the high energy regime where parallel momentum is found to enhance reaction. Gross found that this occurs in a mechanism in which the molecule's momentum is almost parallel to the surface in the minimum barrier regime. If it has enough parallel momentum, it is then able to climb up the maximum barrier (where, strangely enough, most of the reaction occurs) because the propagation direction and the potential gradient are almost aligned.

As discussed by Darling and Holloway,[42] a geometrically corrugated PES leads to a different dependence of reaction on initial parallel momentum. It is also possible that a PES has both geometric and energetic corrugation. If the lowest barriers are furthest away from the surface [as is the case for $H_2+Pt(111)$], essentially the same behavior results as for a PES with pure energetic corrugation.[42]

As mentioned above, the effect of $E_\parallel$ on the reaction probability is largest for the $\langle 11\bar{2}\rangle$ incidence direction: For this direction, increasing $E_\parallel$ from 0.16 to 0.48 eV still has a large effect on reaction. We will now discuss the origin of this more subtle effect. For this, we introduce the term ''reaction plane.'' For each incidence direction, the reaction plane is defined as the plane of incidence (parallel to the incidence direction and perpendicular to the surface) which includes the site with the lowest barrier in it. For $H_2+Pt(111)$, the reaction plane must include the top site. At low-collision energy, reaction will occur in or close to the reaction plane associated with the incidence direction.

We will first discuss the low energy regime ($E_Z<0.20$ eV), in which the reaction dynamics will be determined by the reaction plane. For incidence along the $\langle 10\bar{1}\rangle$ and $\langle 11\bar{2}\rangle$ directions, the reaction planes correspond to the vectors shown in Fig. 5. In the $\langle 10\bar{1}\rangle$ reaction plane, the minimum barrier height is 0.06 eV (top site) and the maximum barrier height is 0.27 eV (bridge site). Taking into account the zero-point energy (ZPE) release for initial $v=0$, the ZPE-corrected barrier heights are 0.04 and 0.21 eV, respectively.[1] In the $\langle 11\bar{2}\rangle$ direction the minimum barrier height is 0.06 eV (top site) and the maximum barrier height 0.42 eV (fcc site). The ZPE-corrected barrier heights are 0.04 and 0.34 eV, respectively. The difference between the minimum and maximum ZPE-corrected barrier height in the reaction plane is indicative of the strength of the energetic corrugation. Let us call this difference E_{corg}. Then, as long as the parallel energy $E_\parallel<E_{\mathrm{corg}}$, we are in the hindering regime. In the $\langle 10\bar{1}\rangle$ reaction plane $E_{\mathrm{corg}}=0.17$ eV, compared to 0.30 eV in the $\langle 11\bar{2}\rangle$ reaction plane, indicating that the energetic corrugation is much larger in the $\langle 11\bar{2}\rangle$ reaction plane than in the $\langle 10\bar{1}\rangle$ reaction plane. This is why there is almost no difference in the reaction probability curves for incidence along the $\langle 10\bar{1}\rangle$ direction in Fig. 5 for $E_\parallel=0.16$ and $E_\parallel=0.48$ eV. Along the $\langle 10\bar{1}\rangle$ direction, a parallel energy of 0.16 eV is almost enough for the molecule to move undisturbed in the reaction plane once it has climbed up the minimum energy barrier. On the other hand, for the $\langle 11\bar{2}\rangle$ incidence direction, reaction is expected to change up to initial parallel energies of 0.30 eV, and this is why we still find large differences between the results for $E_\parallel=0.16$ and $E_\parallel=0.48$ eV.

The differences between the behavior observed in the high-energy regime for $\langle 10\bar{1}\rangle$ and $\langle 11\bar{2}\rangle$ can be explained in an analogous way. The greater the E_{corg}, the greater the range of $E_\parallel$ for which increased $E_\parallel$ will help reaction. This explains the larger differences between the reaction probability curves associated with $E_\parallel=0.16$ and $E_\parallel=0.48$ eV that is observed for the $\langle 11\bar{2}\rangle$ direction.

C. Off-normal incidence: Diffraction

The diffraction probabilities show interesting features that might be confirmed in experiment. In Figs. 6(a) and 6(b) the probability of diffraction into diffraction order P is shown for $P=0-3$, for both incidence directions and an initial parallel translational energy $E_\parallel=0.48$ eV. There is a striking difference in diffraction between the two incidence directions. For incidence along the less corrugated $\langle 10\bar{1}\rangle$ direction [Fig. 6(b)], diffraction into the first-order diffraction is a much more efficient process than for incidence along the more corrugated $\langle 11\bar{2}\rangle$ direction, where specular reflection dominates for low E_Z [Fig. 6(a)]. The first diffraction order consists of six diffraction channels: $(-1,-1)$, $(-1,0)$, $(0,-1)$, (0,1), (1,0), and (1,1) (see Fig. 2). Also shown in Fig. 6(b) is the summed probability of out-of-plane diffraction

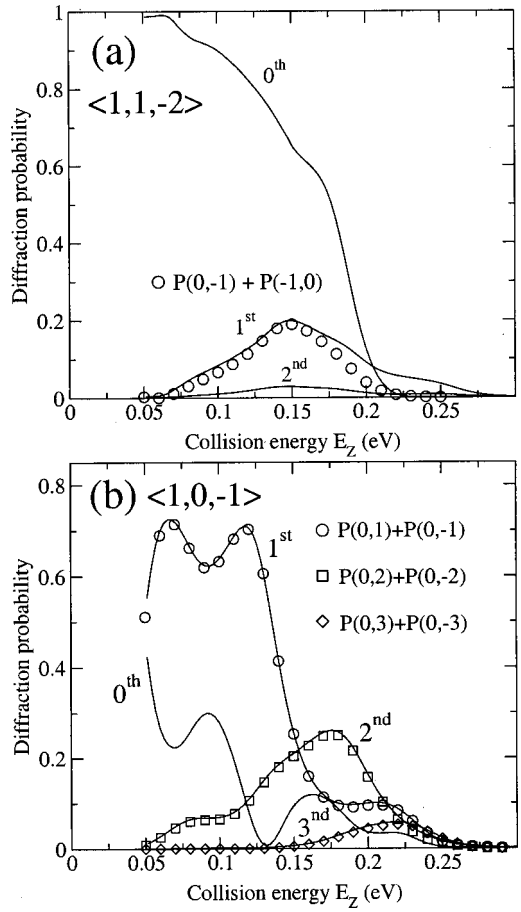

FIG. 6. Shown are the probabilities for diffraction into the zeroth to third diffraction order, for incidence along the $\langle 112\rangle$ (a) and $\langle \bar{1}01\rangle$ (b) direction. The initial parallel energy $E_{\|}=0.48$ eV. Also, for the $\langle 101\rangle$ incidence direction, the summed probability is plotted for diffraction into the diffraction channels $(0,m)$ and $(0,-m)$, that belong to the mth diffraction order and correspond to out-of-plane diffraction. For the $\langle 112\rangle$ incidence direction, we also show the sum of the probabilities for diffraction into the $(0,-1)$ and $(-1,0)$ states.

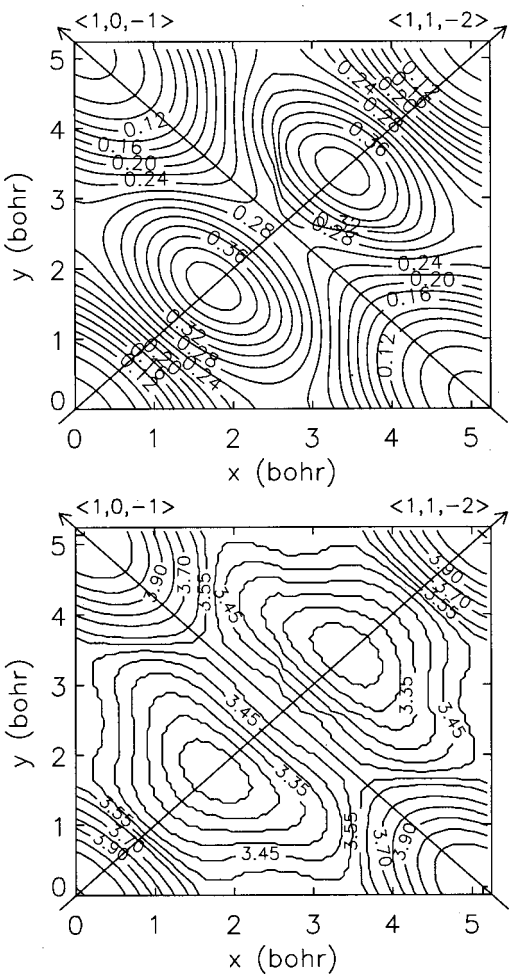

FIG. 7. Contour plots of the barrier height in eV (upper) and distance of the barrier to the surface in bohr (lower) are shown as functions of x and y within the surface unit cell. They correspond to the energetic and geometric corrugation, respectively. Indicated in each plot are the $\langle 101\rangle$ and $\langle 112\rangle$ incidence directions. Note that the coordinate axes are taken orthogonal even though the (111) unit cell is diamond shaped (see text for explanation).

into the equivalent $(0,-m)$ and $(0,m)$ diffraction channels, that belong to the mth diffraction order, and in which the change of parallel momentum is perpendicular to the plane of incidence. For each diffraction order, almost all probability goes into these two out-of-plane diffraction channels. Therefore, the increased first order diffraction observed for incidence along the less corrugated $\langle \bar{1}01\rangle$ direction is due to increased out-of-plane diffraction. For incidence along the $\langle 112\rangle$ direction the summed probability of diffraction into the $(0,-1)$ and $(-1,0)$ channels is also plotted. Up to $E_Z=0.15$ eV, almost all first-order diffraction is into these two channels. For higher E_Z, the (1,0) and (0,1) diffraction channels dominate (not shown).

To understand the difference in diffraction between the two incidence directions, and the origin of the strong out-of-plane diffraction for incidence along $\langle \bar{1}01\rangle$, the barrier height and barrier distance Z to the surface are plotted as a function of the position within the unit cell in Fig. 7. (The assumption implicit in presenting Fig. 7 is that the potential will depend strongly on x and y in the vicinity of the reaction barrier, so that the corrugation associated with the barrier will be the most important feature of the PES affecting the diffraction.) Figure 7 presents a square representation of the diamond shaped (111) unit cell. The sides of the square and the diagonal from the lower right to the upper left corner are all equivalent, and correspond to the $\langle 101\rangle$ direction. The diagonal from the lower left to the upper right corner corresponds to the $\langle 112\rangle$ direction. All first-order diffraction channels indicated in Fig. 2 correspond to a change of parallel momentum in a direction that is equivalent with the $\langle 112\rangle$ incidence direction.

In a $\langle 112\rangle$ reaction plane the energetic and geometric corrugation are strongest, both the barrier height and location showing maximum variation. Therefore, based purely on the strong corrugation along this direction, an incident molecule would be expected to experience the strongest diffraction into a $\langle 112\rangle$ direction, i.e., with the change of the parallel momentum being in a direction of strongest corrugation, regardless of the direction of incidence. This is consistent with our finding that, for incidence along the $\langle 101\rangle$ direction, efficient diffraction occurs into the $(0,-m)$ and $(0,m)$ diffraction channels, which correspond to diffraction into a $\langle 112\rangle$ direction [see Fig. 6(b)].

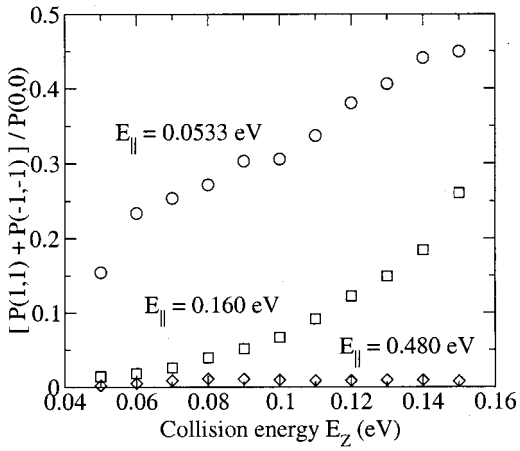

FIG. 8. Plotted is the ratio of first-order in-plane diffraction to specular reflection, for incidence along the $\langle 11\bar{2}\rangle$ direction. The ratio is plotted as a function of the normal collision energy E_Z, for three different initial parallel energies $E_\parallel$.

From a point of view of strong corrugation alone, for incidence along the $\langle 11\bar{2}\rangle$ direction, first-order in-plane diffraction is then expected to occur with large probabilities. But the other four first-order diffraction channels are also expected to occur with a high efficiency. However, Fig. 6(a) demonstrates that first-order diffraction is almost entirely into the out-of-plane $(-1,0)$ and $(0,-1)$ channels. The question then is: Why is diffraction into these out-of-plane channels so much more efficient than in-plane diffraction? This can be understood if one assumes that the diffraction probability is inversely proportional to the energy transferred.[44] The energy transferred in first-order in-plane diffraction equals $(2|\mathbf{K}^0|\Delta k+\Delta k^2)/2m$. Here, $\Delta k=2\pi/(L\sin\gamma)$, and is the minimum amount of momentum that can be gained or lost during the interaction with surface. This expression shows that the energy that needs to be transferred depends on the initial momentum $|\mathbf{K}^0|$: The larger $|\mathbf{K}^0|$, the more energy needs to be transferred, and the smaller the in-plane diffraction probabilities will be. The validity of this assumption is demonstrated in Fig. 8. Shown is the ratio of the sum of in-plane forward and in-plane backward first order diffraction to specular reflection, for three initial parallel energies. Clearly, by increasing $E_\parallel$, and therefore, $|\mathbf{K}^0|$ the probability for in-plane diffraction decreases, showing that the diffraction probability is indeed inversely proportional to the energy transferred. However, this is only true for E_Z upto 0.16 eV. For higher E_Z, the above assumption is no longer valid.

The above analysis shows that one cannot use an argument based on corrugation alone to predict that diffraction will predominantly occur in a particular direction. Just as important is the amount of energy that is transferred in the process.

We can now also understand why, for low E_Z, diffraction occurs almost exclusively into the out-of-plane $(-1,0)$ and $(0,-1)$ channels, for incidence along the $\langle 11\bar{2}\rangle$ direction [Fig. 6(a)]. The energy difference associated with a transition to these channels equals $(|\mathbf{K}^0|\Delta k-\Delta k^2)/2m$, and is much smaller than the energy difference associated with in-plane diffraction. However, the energy difference associated with diffraction into the other two out-of-plan channels, (0,1) and (1,0) is the same, except that in the latter case energy is transferred from motion in Z to motion parallel to the surface, whereas in the former case energy is transferred from parallel motion to motion in Z. It is more likely that, for low E_Z, energy will flow from parallel motion, in which a lot of energy is available ($E_\parallel=0.48$ eV), to motion in Z, where little energy is available. This explains why the (1,0) and (0,1) diffraction channels are not important at low E_Z but only at high E_Z when there is enough energy available in motion in Z.

For incidence along the $\langle 10\bar{1}\rangle$ direction and diffraction into the out-of-plane (0,1) and $(0,-1)$ diffraction channels, the momentum change is perpendicular to the direction of initial motion. The energy change associated with these diffraction channels is small, being equal to $\Delta k^2/2m$, and independent of the initial parallel momentum $\mathbf{K}^0$. The other four first order diffraction channels, all have a momentum component (anti-)parallel to the direction of initial motion (see Fig. 2). The energy change associated with transitions to these channels, therefore, involves a term dependent on $|\mathbf{K}^0|$, and with $|\mathbf{K}^0|$ being quite large ($E_\parallel=0.48$ eV), the extra energy needed explains why these channels contribute almost nothing to the total first-order diffraction [Fig. 6(b)].

One of the most important observations for $E_\parallel=0.48$ eV is that, for both incidence directions, in-plane diffraction (which is the diffraction that was observed in experiment) is unimportant compared to out-of-plane diffraction. The other important observation is that, for the $\langle 11\bar{2}\rangle$ incidence direction, specular reflection is much more important than first-order diffraction, because for all six first order diffraction channels, the corresponding momentum change has a component along the incidence direction, leading to a large energy gap for diffraction into these channels, at $E_\parallel=0.48$ eV.

For $E_\parallel=0.16$ eV, the results are very similar to those of $E_\parallel=0.48$ eV. Even for $E_\parallel=0.0533$ eV, there is a clear preference for the first-order out-of-plane diffraction into the $(0,-1)$ and (0,1) diffraction channels for incidence along the $\langle 10\bar{1}\rangle$ direction. However, for incidence along the $\langle 11\bar{2}\rangle$ direction and $E_\parallel=0.0533$ eV, diffraction into the out-of-plane $(-1,0)$ and $(0,-1)$ diffraction channels is far more efficient than for $E_\parallel=0.48$ eV, and the total probability of first order diffraction is larger than specular reflection, for $E_Z<0.16$ eV.

D. Comparison with experiment: Reaction

In Fig. 9 the computed dissociation probability is compared with molecular beam results of Luntz *et al.*[11] for D_2. The computed reaction probability is plotted as a function of the total incidence energy E_i for different initial parallel momenta of H_2 along the $\langle 10\bar{1}\rangle$ direction. The incidence direction used in the experiment is not known. This probably does not hinder the comparison to experiment: The reaction probabilities computed do not differ much for $\vartheta_i=0°$, 30°, and 45° and the two incidence directions we considered; only for $\vartheta_i=60°$ large differences were calculated. The sticking probabilities of Luntz *et al.* were also presented as a function

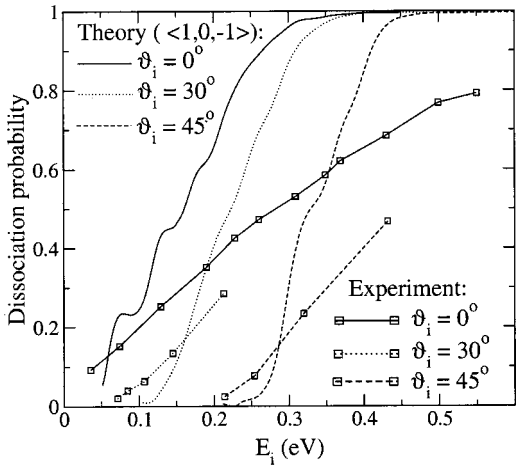

FIG. 9. Results of 4D quantum calculations for normal and off-normal incidence are compared with experimental results by Luntz *et al.* for $D_2 + Pt(111)$.[11] Curves associated with equal ϑ_i should be compared.

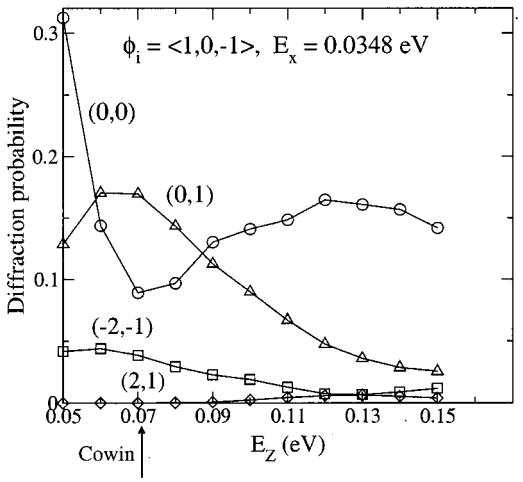

FIG. 10. In-plane diffraction probabilities for the lowest order forward (2,1) and backward $(-2,-1)$ diffraction channels are compared with the specular scattering probability. For a normal collision energy $E_Z \approx 0.07$ eV (arrow below axis), the experimental conditions of Cowin *et al.* (Ref. 12) are almost exactly reproduced. Also plotted is the out-of-plane diffraction probability for diffraction into the (0,1) channel, which is equivalent to the $(0,-1)$ channel.

of the total incidence energy E_i, but for fixed polar angles of incidence θ_i. From their data we extracted combinations of E_i and θ_i that correspond to combinations of E_Z and $E_\parallel$ (or ϑ_i) in our calculations. Note that comparing our theoretical data for H_2 with experimental data for D_2 should be justified: Luntz *et al.* could not detect a measurable isotope effect in their experiments on reaction of H_2 and D_2 on Pt(111).

The comparison shows that the onset of the reaction probabilities agrees quite well with experiment, but that for higher energies the 4D calculation predicts much higher reaction probabilities. The same conclusions were drawn for the 3D calculations.[1] In both the previous 3D and the present 4D calculations, the molecule is fixed in its most favorable orientation for dissociation, namely the parallel orientation. This explains the agreement for energies just above the onset energy. Including rotation is expected to reduce the probability for higher energies due to the presence of unfavorable molecular orientations.

E. Comparison with experiment: Diffraction

In experiments by Cowin *et al.*[12] on rotational inelastic scattering of HD from Pt(111) a very small probability of first order in-plane diffraction was found. Their conclusion was that the HD+Pt(111) potential is only very weakly corrugated. Yet, Luntz *et al.*[11] found that normal energy scaling was not obeyed, suggesting a rather corrugated potential. The conclusions by Luntz are supported by the PES calculated from DFT[36,38] and the results of calculations for reaction probabilities presented in Fig. 5. Figure 10 also shows calculated probabilities of specular reflection and first order in-plane forward and in-plane backward diffraction, into the (2,1) and $(-2,-1)$ diffraction channels, respectively. (Although these diffraction channels are of second order according to our definition, as illustrated in Fig. 2, they correspond to the lowest order in-plane diffraction channels, and are therefore, referred to as first-order in-plane diffraction channels by experimentalists.) The molecule is incident along the $\langle 10\bar{1} \rangle$ direction with an initial parallel translation energy equal to 0.0348 eV ($\vartheta_i = 25°$). For this energy, the experimental conditions of Cowin *et al.* for the $\langle 10\bar{1} \rangle$ incidence direction ($\theta_i = 35°, E_i = 109$ meV) are almost exactly reproduced at the normal energy indicated by the arrow below the *x* axis. Although Cowin repeated the experiment for angles θ_i ranging from 20° to 85°, only for $\theta_i = 35°$ results were shown in a detailed plot (see Fig. 3 of Ref. 12). In disagreement with the experiment, the amount of diffraction into the $(-2,-1)$ channel is still fairly large when compared to the specular channel.

For normal energies below the energy used by Cowin *et al.* in Fig. 10, the ratio of specular scattering to the $(-2,-1)$ diffraction channel increases quite rapidly. For instance, lowering the normal energy from 0.07 to 0.05 eV (which corresponds to an increase of θ_i from 35° to 40°) leads to a large increase in this ratio (from 2.3 to 7.5). These normal energies correspond to the onset of reaction. In this regime, the diffraction and reaction are going to be quite sensitive to the rotations of the molecule. For instance, due to orientational averaging over the potential a molecule approaching in $j = 0$ would be able to come less close to the surface at these energies, resulting in less reaction and diffraction. Therefore, we would expect to see a higher ratio of specular scattering to in-plane diffraction in 6D calculations performed for off-normal incidence, in better agreement with experiment. The sensitivity of the ratio (specular scattering/lowest order in-plane diffraction) to normal incidence energy which is here observed at the onset of reaction, suggests this quantity to be a sensitive probe of the minimum barrier height.

For an incidence angle $\theta_i = 45°$ and a total incidence energy $E_i = 111$ meV, Cowin *et al.*[12] found that the ratio (specular reflection/lowest order in-plane diffraction) is about 100 for the $\langle 10\bar{1} \rangle$ direction, and about 10 for the $\langle 11\bar{2} \rangle$ incidence direction. Under these conditions the initial parallel energy and normal energy are both equal to 55.5 meV, making a quantitative comparison with our calculation for

$\vartheta_i = 30°$ ($E_\parallel = 53.3$ meV) possible. For the $\langle 10\bar{1} \rangle$ direction we find a computed ratio of about 18, and for the $\langle 11\bar{2} \rangle$ incidence direction about 6. (These numbers were obtained by interpolating the computed ratios for 0.05 and 0.06 eV.) The computed ratio for the $\langle 10\bar{1} \rangle$ direction is too small by a factor 5.5. However, in a 6D calculation, this ratio is expected to increase as indicated above. For the $\langle 11\bar{2} \rangle$ direction the computed ratio is already in reasonable agreement with the experimental ratio (6 versus 10).

By correcting for the Debye–Waller attenuation and geometrical losses, Cowin *et al.*[12] obtained absolute rotational excitation probabilities for zero-order diffraction. Summing the rotationally (in)elastic zero-order diffraction probabilities, they found that the summed probability could not account for all the probability. For instance, for incidence along the $\langle 10\bar{1} \rangle$ direction, and $\theta_i = 35°$ and 45°, and $E_i = 109$ and 110 meV, they found a summed probability of 0.257 and 0.281, respectively. These conditions are (almost) reproduced by our calculations for ϑ_i equal to 25° and 30°. We find a zero-order diffraction probability of 0.088 and 0.34, respectively. Cowin *et al.* tried to account for the missing probability by estimating the total nonzero-order diffraction probability, assuming that diffraction is roughly independent of the incidence direction. This assumption led them to conclude that nonzero-order diffraction is only about one third of the zero-order diffraction, suggesting that nonzero-order diffraction could not account for the missing probability.[12] However, our calculations show that for the $\langle 10\bar{1} \rangle$ incidence direction, the nonzero-order diffraction probability is 0.87 for $\theta_i = 35°$, and 0.57 for $\theta_i = 45°$. First order in-plane diffraction is responsible for only a small fraction, $<5\%$, of the total probability, suggesting that out-of-plane diffraction is responsible for much of the missing probability observed by Cowin *et al.*, and much more important than suggested by them.[12]

As already explained, at off-normal incidence out-of-plane diffraction is much more important than in-plane diffraction. At the energy and polar angle of incidence ($\theta_i = 35°, E_i = 109$ meV) for which Cowin *et al.* provided a plot of their results, out-of-plane diffraction is quite efficient. This is also shown in Fig. 10, by plotting the (0,1) probability for diffraction perpendicular to the plane of incidence. The total probability for first-order diffraction (6 out-of-plane channels) is 0.50 at the experimental conditions of Cowin *et al.*, and the total probability for second-order diffraction (12 channels) is 0.25 [compared to 0.038 for the two in-plane diffraction channels, of which the (2,1) channel is closed at these conditions]. For normal incidence, the total first-order diffraction probability is only 0.031 at the same normal collision energy E_Z, suggesting that it is the hindering of reaction by initial parallel motion that leads to the large amount of out-of-plane diffraction here observed.

Our previous 3D calculations for off-normal incidence along $\langle 11\bar{2} \rangle$ showed very large probabilities for first order in-plane diffraction (larger than for specular scattering) at the experimental conditions of Cowin *et al.* Our present 4D calculations show that the ratio (specular scattering/lowest order in-plane diffraction) is much increased by competition with out-of-plane diffraction. We believe this represents an important piece of the puzzle posed by the paradox presented by the experimental results for reaction and diffraction. Part of the reason that the surface seems flat in experiments on diffraction is that the experiments performed so far could only observe in plane diffraction, and not the substantial out-of-plane diffraction here predicted. This substantial out-of-plane diffraction is proof of a corrugated surface, as is the observation that reaction does not obey normal energy scaling, as found in the experiments of Luntz *et al.*[11] We expect that the other pieces of the puzzle have to do with rotational effects (as will be probed in the 6D calculations we are performing), and possibly with the fact that Cowin *et al.* looked at scattering of HD whereas we model scattering of H_2.

The above analysis clearly suggests that the ratio (specular scattering/lowest order in-plane diffraction) is not a reliable quantity for assessing the amount of corrugation of the $H_2 + Pt(111)$ system. Both incidence directions here considered have disadvantages for obtaining insight in the amount of corrugation by looking at in-plane diffraction. The $\langle 10\bar{1} \rangle$ direction is the least corrugated direction, and the lowest order in-plane diffraction channels are of order 2 (see Fig. 2), requiring a larger momentum transfer. Both factors are unfavorable for diffraction. In addition, for incidence along the $\langle 10\bar{1} \rangle$ direction, out-of-plane diffraction along the $\langle 11\bar{2} \rangle$ direction can be expected (and is seen) to out-compete the in-plane diffraction. The $\langle 11\bar{2} \rangle$ direction should be most favorable for observing diffraction, because it is the most corrugated direction, and the lowest order in-plane diffraction channels are of order 1 (see Fig. 2). Nevertheless, even for this direction we compute much more out-of-plane diffraction than in-plane diffraction, suggesting that experiments which only measure in-plane diffraction can only provide limited information on the corrugation of the PES for $H_2 + Pt(111)$.

In summary, to prove the corrugated nature of the $H_2 + Pt(111)$ PES in a diffraction experiment, one should consider incidence along the $\langle 10\bar{1} \rangle$ direction and measure the first order out-of-plane diffraction channels that correspond to a momentum change perpendicular to the incidence direction. Our results show that for collision energies $0.05\ \text{eV} < E_Z < 0.125\ \text{eV}$, and for angles of incidence $\theta_i \geqslant 35°$, first order out-of-plane diffraction into the (0,1) and (0,−1) channels occurs with large probabilities, and are much more important than in-plane diffraction. It should be possible to measure out-of-plane diffraction for such conditions using existing experimental techniques.[45–47]

IV. CONCLUSION

A time-dependent wave packet (TDWP) method has been used to study the dissociative and diffractive scattering of H_2 from Pt(111) within a four-dimensional (4D) model. The work presented here is an extension of earlier, three-dimensional calculations on the same system.[1] An important motivation for this research is a paradox concerning the degree of corrugation of the potential energy surface (PES) and its effect on dissociation and diffraction. Molecular beam experiments looking at reaction $(H_2, D_2 + Pt(111))$[11]

and rotationally inelastic and diffractive scattering (HD+Pt(111))[12] came to opposite conclusions regarding the amount of corrugation of the PES.

In the 4D calculations the molecule is kept parallel to the surface, and has freedom in motion normal to the surface, in the internuclear distance and in two directions parallel to the surface. A 4D PES is used that is the result of an interpolation of four 2D PESs. Each 2D PES is calculated with density-functional theory (DFT), using the generalized gradient approximation (GGA) and a slab representation of the surface.[36]

As summarized below, the 4D calculations offer important new insights in the diffraction of H_2 on Pt(111). However, the results of the 4D calculations do not alter any of the major conclusions from previous 3D calculations concerning reaction. We again find a large vibrational enhancement of reaction for $v=1$ H_2 compared with $v=0$ H_2, which is not due to a reduced mass[14] effect, all barriers being early, but to a decrease of the force constant of the H_2 vibration as the molecule approaches the barrier.[1,15]

Calculations have also been done for various incidence angles and two incidence directions. The results show that normal energy scaling is not obeyed, in agreement with experiment.[11] The effect of initial parallel momentum depends on the translational energy normal to the surface E_Z. For low E_Z parallel momentum inhibits dissociation which is due to the molecules scattering off high barriers as they move parallel to the surface.[42,43] The higher the initial parallel momentum, the more likely that the molecule will encounter a high barrier and scatter back into the gas phase. A new result of the 4D calculations is that the more corrugated the potential is along a specific incidence direction, the larger the range of initial parallel momentum is for which reaction continues to be hindered, at low normal energies.

A quantitative comparison of the 4D computed reaction probability with previous 3D results show good agreement between 4D and 3D. At low energies the 4D reaction probability is somewhat lower than in 3D, and at high energies the 4D model is more reactive. These differences can be understood qualitatively by using a hole model analysis. The 3D model is more reactive at low energies because the lowest barrier site has a higher statistical weight in 3D, and it is less reactive at high energies because the highest barrier site also has a higher statistical weight in the 3D model.

A comparison was made with experimental results. The dissociation onset is, as for the 3D model, in good agreement with experiment. For higher energies, though, there is a large discrepancy between theory and experiment. This is not unexpected because in the 4D calculations the molecule is always parallel to the surface. Including rotation is expected to lead to smaller reaction probabilities due to the presence of unfavorable orientations.

Molecular beam experiments by Cowin *et al.*[12] for off-normal angles of incidence ranging from 25 to 80 degrees from the normal and total energies of about 110 meV show very little in-plane diffraction, suggesting that the H_2 +Pt(111) PES is rather flat. The present 4D calculations, in which an additional degree of freedom for parallel motion was introduced compared to previous 3D calculations modeling only one diffractive degree of freedom, show that, for off-normal incidence along the $\langle 101 \rangle$ incidence direction, out-of-plane diffraction (which the experiments did not look at) is much more important than in-plane diffraction. Competition with out-of-plane diffraction leads to a large decrease of in-plane diffraction. This sheds new light on the paradox posed by previous experiments on reaction of H_2 on Pt(111) and scattering of HD from Pt(111). The scattering experiments failed to observe evidence for the corrugation of the surface (as also presented by the experiments on reaction) because they failed to observe out-of-plane diffraction, in which the corrugation should be most manifest. Our results suggest that proof of the corrugation of the H_2 +Pt(111) system can be found in first order out-of-plane diffraction for incidence along the $\langle 101 \rangle$ direction. In that case one must look at the first-order diffraction channels that correspond to a momentum change perpendicular to the incidence direction. These channels occur with probabilities much larger than in-plane diffraction. If the experiments that we propose confirm our predictions, they will show that the paradox alluded to above is in fact a false contradiction: The scattering experiments failed to find proof of the corrugation of the surface because out-of-plane diffraction was not considered.

ACKNOWLEDGMENTS

Authors E.P. and G.J.K. gratefully acknowledge the Stichting Nationale Computerfaciliteit (NCF) for generous grants of computation time. Authors R.A.O. and E.J.B. are grateful for funding by the National Research School Combination ''Catalysis by Design.'' Useful discussions with J. P. Toennies, D. Farías, M. F. Bertino, and Y. Ekinci are acknowledged. The authors are also grateful to Professor E. F. van Dishoeck for carefully reading the manuscript.

[1] E. Pijper, G. J. Kroes, R. A. Olsen, and E. J. Baerends, J. Chem. Phys. **113**, 8300 (2000).
[2] S. L. Bernasek and G. A. Somorjai, J. Chem. Phys. **62**, 3149 (1975).
[3] I. E. Wachs and R. J. Madix, Surf. Sci. **58**, 590 (1976).
[4] M. Salmeron, R. J. Gale, and G. A. Somorjai, J. Chem. Phys. **67**, 5324 (1977).
[5] K. Christmann, G. Ertl, and T. Pignet, Surf. Sci. **54**, 365 (1976).
[6] K. Christmann and G. J. Ertl, Surf. Sci. **60**, 365 (1976).
[7] B. Poelsema, L. K. Verheij, and G. Comsa, Surf. Sci. **148**, 117 (1984).
[8] K. Lenz, Berichte der Kernforschunglang Jülich, No. 2141 (1987).
[9] L. K. Verheij, M. B. Hugenschmidt, A. B. Anton, B. Poelsema, and G. Comsa, Surf. Sci. **210**, 1 (1989).
[10] P. Samson, A. Nesbitt, B. E. Koel, and A. Hodgson, J. Chem. Phys. **109**, 3255 (1998).
[11] A. C. Luntz, J. K. Brown, and M. D. Williams, J. Chem. Phys. **93**, 5240 (1990).
[12] J. P. Cowin, C. F. Yu, S. J. Sibener, and L. Wharton, J. Chem. Phys. **79**, 3537 (1983).
[13] G. R. Darling and S. Holloway, Rep. Prog. Phys. **58**, 1595 (1995).
[14] D. Halstead and S. Holloway, J. Chem. Phys. **93**, 2859 (1990).
[15] A. Gross and M. Scheffler, Chem. Phys. Lett. **256**, 417 (1996).
[16] R. Kosloff, J. Phys. Chem. **92**, 2087 (1988).
[17] A. D. Becke, Phys. Rev. A **38**, 3098 (1988).
[18] J. P. Perdew, Phys. Rev. B **33**, 8822 (1986).
[19] G. te Velde and E. J. Baerends, Phys. Rev. B **44**, 7888 (1991).
[20] G. J. Kroes, Prog. Surf. Sci. **60**, 1 (1999).
[21] A. Gross, Surf. Sci. Rep. **32**, 291 (1998).
[22] J. Dai and J. C. Light, J. Chem. Phys. **107**, 1676 (1997).
[23] E. Pijper, Ph.D. thesis.

[24] R. C. Mowrey and G. J. Kroes, J. Chem. Phys. **103**, 1216 (1995).
[25] A. Vibók and G. G. Balint-Kurti, J. Chem. Phys. **96**, 7615 (1992).
[26] M. D. Feit, J. J. A. Fleck, and A. Steiger, J. Comput. Phys. **47**, 412 (1982).
[27] G. G. Balint-Kurti, R. N. Dixon, and C. C. Marston, J. Chem. Soc., Faraday Trans. **86**, 1741 (1990).
[28] C. C. Marston, G. G. Balint-Kurti, and R. N. Dixon, Theor. Chim. Acta **79**, 313 (1991).
[29] G. G. Balint-Kurti, R. N. Dixon, and C. C. Marston, Int. Rev. Phys. Chem. **11**, 317 (1992).
[30] J. C. Light, I. P. Hamilton, and J. V. Lill, J. Chem. Phys. **82**, 1400 (1985).
[31] N. W. Ashcroft and N. D. Mermin, *Solid State Physics* (Philadelphia, Saunders College, 1976).
[32] C. Kittel, *Introduction to Solid State Physics* (Wiley, New York, 1986).
[33] G. J. Kroes and R. C. Mowrey, J. Chem. Phys. **101**, 805 (1994).
[34] G. J. Kroes, J. G. Snijders, and R. C. Mowrey, J. Chem. Phys. **103**, 5121 (1995).
[35] G. te Velde and E. J. Baerends, Chem. Phys. **177**, 399 (1993).
[36] R. A. Olsen, G. J. Kroes, and E. J. Baerends, J. Chem. Phys. **11**, 11155 (1999).
[37] P. H. T. Philipsen, E. van Lenthe, J. G. Snijders, and E. J. Baerends, Phys. Rev. B **56**, 13556 (1997).
[38] R. A. Olsen, H. F. Busnengo, A. Salin, M. F. Somers, G. J. Kroes, and E. J. Baerends, J. Chem. Phys. **116**, 3841 (2002).
[39] D. Neuhauser and M. Baer, J. Chem. Phys. **91**, 4651 (1989).
[40] J. Harris, Surf. Sci. **221**, 335 (1989).
[41] G. R. Darling and S. Holloway, Surf. Sci. **307–309**, 153 (1994).
[42] G. R. Darling and S. Holloway, Surf. Sci. **304**, L461 (1994).
[43] A. Gross, J. Chem. Phys. **102**, 5045 (1995).
[44] R. D. Levine and R. B. Bernstein, *Molecular Reaction Dynamics and chemical Reactivity* (Oxford University Press, Oxford, 1987).
[45] J. P. Toennies, in *Surface Phonons*, edited by W. Kress and F. W. de Wette, Springer Series in Surface Science (Springer, Berlin, 1991), Vol. 21, p. 111.
[46] J. R. Buckland and W. Allison, J. Chem. Phys. **112**, 970 (1999).
[47] D. Farías and K. H. Rieder, Rep. Prog. Phys. **61**, 1575 (1998).